Editors' Suggestion | Featured in Physics

Multifractal Conductance Fluctuations in High-Mobility Graphene in the Integer Quantum Hall Regime

Kazi Rafsanjani Amin,* Ramya Nagarajan, Rahul Pandit, and Aveek Bid†
Department of Physics, Indian Institute of Science, Bangalore, Karnataka 560012, India

(Received 3 January 2022; revised 9 June 2022; accepted 15 September 2022; published 26 October 2022)

We present the first experimental evidence for the multifractality of a transport property at a topological phase transition. In particular, we show that conductance fluctuations display multifractality at the integer quantum Hall plateau-to-plateau transitions in high-mobility mesoscopic graphene devices. The multifractality gets rapidly suppressed as the chemical potential moves away from these critical points. Our combination of experimental study and multifractal analysis provides a novel method for probing the criticality of wave functions at phase transitions in mesoscopic systems, and quantum criticality in several condensed-matter systems.

DOI: 10.1103/PhysRevLett.129.186802

Since its discovery, the integer quantum Hall (IQH) effect, a continuous quantum-phase transition in a two-dimensional electron gas (2DEG) [1], has provided us with a paradigm for topological phase transitions. In the presence of a large magnetic field B, applied perpendicular to the surface, the density of states (DOS) of a noninteracting 2DEG develops into discrete, quantized Landau levels. Disorder broadens these degenerate Landau levels into bands of extended states separated by localized states. When the Fermi level E_F, tuned by changing either B or the charge-carrier density n, lies in the localized states [cf. Fig. 1(a)], the Hall conductance G_{XY} is quantized in units of e^2/h, and the transverse conductance G_{XX} becomes vanishingly small, with $G_{XX} = 0$ at a temperature $T = 0$ [2]. In this regime, transport takes place through chiral edge modes, whose number is dictated by the topological Chern number of the system [3–6]. If, by contrast, E_F lies in the range of energies at the center of the Landau levels, transport proceeds through the bulk with $G_{XX} \neq 0$ and a nonquantized G_{XY}.

The Hall conductivity at a given point depends strongly on the disorder potential and the local DOS (LDOS) over a length scale of the order of the localization length ξ [17–22]. Central to this argument is the idea that IQH plateau-to-plateau transitions are localization-delocalization transitions across the mobility edge [23–26]. This observation, in turn, has significant implications for modern theories of IQH that acknowledge the effect of local perturbations on such topological phase transitions [27,28].

The eigenstates at the mobility edge are *critical* and different from those in both localized and extended states [23,29–31]. As the Landau-level filling factor ν approaches its critical value, the localization length ξ diverges algebraically as $\xi \propto |\nu - \nu_C|^{-\gamma}$. Theoretical studies show that observables like the distribution of the local density squared $|\psi(\mathbf{r})|^2$ [23,32] or the equilibrium current density squared $|j(\mathbf{r})|^2$ [33] display multifractal fluctuations leading to anomalous diffusion [26] and, consequently, a power-law decay of the density correlations, a slow decay of temporal wave-packet autocorrelations [34] and, most significantly for our purpose, multifractal conductance fluctuations [35–39].

In this Letter, we present the first experimental evidence for the multifractality of a transport property at a topological phase transition [3–6]. In particular, we show that, in high-mobility graphene at the IQH plateau-to-plateau transitions, the conductance fluctuations are multifractal. The origin of this multifractality may be understood by noting that as IQH criticality is approached, the LDOS penetrates the bulk of the material from its edges, and a complex hierarchical distribution emerges. This distribution is governed by the multifractal wave functions and results in the multifractality of Hall conductance at criticality [22]. Earlier studies on high-mobility GaAs/AlGaAs heterostructures have shown that IQH transitions are accompanied by large, reproducible fluctuations in both G_{XX} and G_{XY} as functions of B and n [21,40,41]. Despite an expectation that a multifractal analysis of these fluctuations is essential for a complete description of the criticality in IQH regimes [23,34], experimental confirmation of this multifractality has been missing hitherto. Our results address this vital lacuna. Our approach of probing the criticality is not limited to studying mesoscopic fluctuations. It can be suitably applied to probe a wide range of systems such as superconductors and topological insulators.

Multifractality, initially introduced to characterize the statistical properties of fluid turbulence [42,43], was later studied in a variety of fields ranging from heartbeats to cloud structures [44–52]. In condensed-matter science,

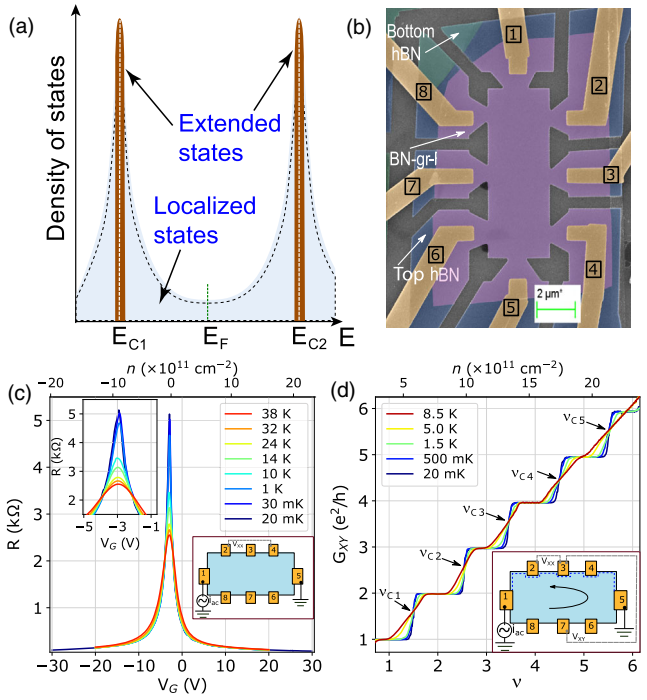

FIG. 1. (a) A schematic diagram illustrating the dependence of the DOS of 2DEG on energy in the IQH regime. The extended states (brown regions) at the centers of the disorder-broadened Landau levels are separated by the localized regions (light blue). The quantum phase transitions between the localized and extended states occur at the mobility edge around the critical energies E_{C1} and E_{C2}. (b) A false-color SEM image of device 1DC8. (c) Plots showing the dependence of R on V_G at different temperatures for 1DC8. The measurements were carried out at $B = 0$ T. The left inset shows an enlarged plot near the Dirac point [see Supplemental Material [7], S2]. The inset at the right indicates the contacts used in the measurement. (d) Plots of G_{XY} versus the filling factor ν measured at different temperatures and magnetic field $B = 16$ T for 1DC8. The arrows mark the positions of IQH critical points at which the localization-delocalization transitions occur. Inset: the contacts used in the measurement. The arrow indicates the chirality of electron transport at $B = 16$ T. The corresponding number density n is given on the top axis of (c) and (d).

most investigations of multifractality, which manifests itself at some phase transitions, employ a combination of theoretical and numerical techniques [36–38,53–57]. The experimental characterizations of multifractality in such condensed-matter settings require precision experiments in high-quality samples, often at very low temperatures. Two recent examples of such measurements are the study of multifractal conductance fluctuations at low magnetic fields [35] and the study of multifractal superconductivity in the weak-disorder regime [58,59].

Our electrical-transport measurements were carried out on hexagonal boron nitride (hBN) encapsulated graphene devices with one-dimensional ohmic contacts—for details, see Supplemental Material [7], S1. The electrical-transport measurements were carried out in a dilution refrigerator, with a base temperature of 20 mK, by using low-frequency lock-in measurement techniques in a multiprobe configuration at a low bias current ($\lesssim 1$ nA) to avoid Joule heating (Supplemental Material [7], S2]. We focus primarily on our data from two devices: 1DC8 and B15D4 (Supplemental Material [7], S3). The samples were thermally cycled multiple times; the data we present did not change significantly on thermal cycling.

In Fig. 1(c), we present plots of the longitudinal resistance R versus the back-gate voltage V_G, measured at $B = 0$ and different values of T for device 1DC8. The field-effect mobility, estimated at $T = 20$ mK, is $\mu = 128\,000$ cm^2 V^{-1} s^{-1}. The corresponding data for device B15D4 are in the Supplemental Material [7], S3.

Figure 1(d) shows plots of G_{XY} versus $\nu(= nh/eB)$ at different temperatures T and at $B = 16$ T for 1DC8. Here, n is the charge carrier density, h is the Planck constant, and e is the electronic charge. Focusing on the data for $T = 20$ mK, we observe well-developed plateaus in G_{XY} at all integer multiples of e^2/h, indicating a complete lifting of the layer, spin, and valley degeneracies of the Landau-level spectra [60,61]. For any one of the transitions between two adjacent plateaus, the plots of G_{XY} versus ν, measured at different temperatures, intersect at a single point in the (ν, G_{XY}) plane. We identify each intersection as the critical point for the quantum phase transitions from localized to delocalized states [24].

To obtain the detailed fluctuation profiles and to investigate their statistics, fine-sweep measurements were performed with a much-reduced step size (250 times higher resolution), in either B or V_G. In Figs. 2(a) and 2(b), we show plots of G_{XY} versus ν, for the $\nu = 1 \leftrightarrow \nu = 2$ IQH transition, at $T = 20$ mK measured with a very small step size in either B or in V_g for 1DC8 (Supplemental Material [7], S4). We find large fluctuations in G_{XY} across the plateau-to-plateau transition. The reproducibility of these fluctuations [Fig. 2(c)] establishes them to be mesoscopic fluctuations with a unique magnetofingerprint. Although these fluctuations remain reproducible over a particular thermal cycle, their detailed profile changes if the device is thermally cycled to $T > 10$ K and back.

We obtain the conductance fluctuations $G'_{\square}(x)$ by subtracting a smooth background from the measured data using $G'_{\square}(x) = G_{\square}(x) - F[G_{\square}(x)]$. Here, x is either B or V_G, $G_{\square}$ stands for G_{XX} or G_{XY}, and the function $F[G_{\square}(x)]$ is the smooth background in $G_{\square}(x)$ (Supplemental Material [7], S4). In this Letter, we discuss the multifractality of G_{XY}; the multifractal spectra of G_{XX} are quantitatively similar (Supplemental Material [7], S8).

In Fig. 2(d), we show representative plots of G'_{XY} versus B, across the $\nu = 1 \leftrightarrow \nu = 2$ transition on device 1DC8, for different values of T and at a fixed value of $n = 4.75 \times 10^{11}$ cm^{-2}. With increasing T, the mean amplitude of the fluctuations in G'_{XY} decreases, but the

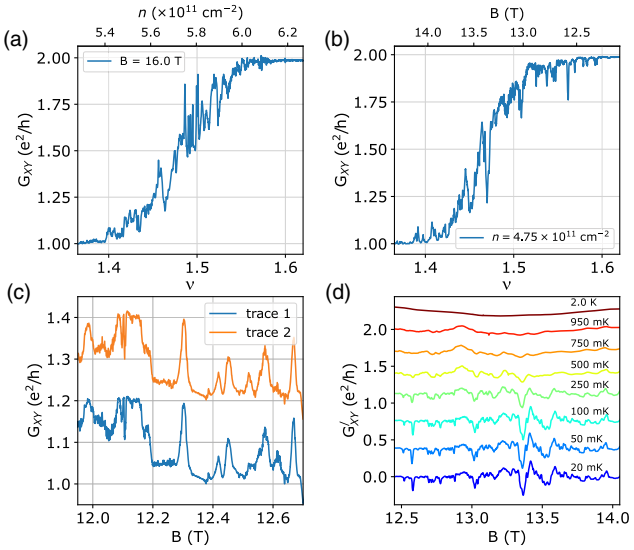

FIG. 2. Plots of G_{XY} versus ν measured during $\nu = 1 \leftrightarrow \nu = 2$ IQH transition at (a) a fixed value of the magnetic field $B = 16$ T and (b) a fixed number density $n = 4.75 \times 10^{11}$ cm^{-2} for the device 1DC8. The corresponding values of n are shown on the top axes. (c) Plots of two different traces of G_{XY} versus B, measured between $\nu = 1.64$ and $\nu = 1.54$, showing the reproducibility of the mesoscopic conductance fluctuations. The datasets have been shifted vertically for clarity. (d) Plots of segments of data of G'_{XY} versus B, for the $\nu = 1 \leftrightarrow \nu = 2$ transition, measured at different temperatures T and at a fixed carrier density $n = 4.75 \times 10^{11}$ cm^{-2}. The data have been vertically offset for clarity. The data presented in (c) are from a different cooldown cycle than those in (a), (b), and (d).

magnetofingerprint of mesoscopic fluctuations persists; these signatures finally become smaller than the measurement-noise level for $T > 1$ K. Although these fluctuations in G'_{XY} disappear for $T > 1$ K, the plateaus of G_{XY}, at e^2/h and $2e^2/h$, survive until much higher temperatures [Fig. 1(b)].

Having established the mesoscopic origin of the fluctuations in the conductance across the plateau-to-plateau transitions, we now analyze the multiscaling behavior and statistics of the fluctuations in the vicinity of the $\nu = 1 \leftrightarrow \nu = 2$ critical points. Our multifractal analysis of these fluctuations is akin to the analysis in our previous low-field study of universal conductance fluctuations in single-layer graphene [35] (Supplemental Material [7], S5). Briefly, the G'_{XY} data series is divided into several segments, each centered at different values of the filling factor ν. We then compute the multifractal spectrum as follows: each such segment is detrended and subdivided into N_s overlapping segments, indexed by j, and containing s data points, with $1 \le j \le N_s$. The generalized Hurst exponents $h(q)$ are obtained from the power-law-scaling behavior of the order-q moment of the fluctuations $F_q(s)$ using the following relations:

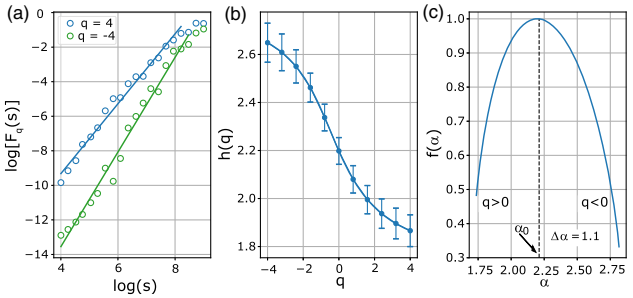

FIG. 3. (a) Plots of $\log[F_q(s)]$ versus $\log[s]$ [see Eq. (2)], for $q = -4$ (green circles) and $q = 4$ (blue circles) for a typical data segment of G'_{XY}. The thick lines are the linear fits to the data points. (b) Plot of $h(q)$ versus q for the data segment shown in (a). (c) Plot of the singularity spectrum $f(\alpha)$ versus α obtained from (b). The maximum value of this spectrum is $f_{\max}(\alpha) = 1$ located at $\alpha_0 \simeq 2.21$ (marked by an arrow). The data were obtained at $\nu = 1.47$ and 20 mK for the device 1DC8.

$$g_{\rm rms}(j) = \left[\frac{1}{s}\sum_{i=1}^{s}(g_i)^2\right]^{1/2}; \tag{1}$$

$$F_q(s) = \left[\frac{1}{N_s}\sum_{j=1}^{N_s} g_{\rm rms}(j)^q\right]^{1/q} \sim s^{h(q)}. \tag{2}$$

A q-dependent $h(q)$ indicates multifractality. That this is indeed the case for G_{XY} measured across the $\nu = 1 \leftrightarrow \nu = 2$ transition can be clearly seen from the different slopes of the $\log[F_q(s)]$ versus $\log(s)$ plots for $q = \pm 4$ in Fig. 3(a) and from the plot of $h(q)$ versus q in Fig. 3(b). For similar plots establishing the multifractality of the $\nu = 2 \leftrightarrow \nu = 3$ transition, the multifractality of G_{XX}, and for data on device B15D4, see the Supplemental Material [7].

Multifractality can be represented by the singularity spectrum, which is a plot of $f(\alpha)$ versus α obtained by the Legendre transformation of $h(q)$ as follows:

$$\alpha = h(q) + qh'(q),$$
$$f(\alpha) = q[\alpha - h(q)] + 1. \tag{3}$$

In Fig. 3(c), we show a plot of $f(\alpha)$, obtained at 20 mK near the $\nu = 1 \leftrightarrow \nu = 2$ critical point; the data obtained for the $\nu = 2 \leftrightarrow \nu = 3$ critical transition are qualitatively similar (Supplemental Material [7], S13). The large width of $f(\alpha)$, $\Delta\alpha \simeq 1.1$ indicates significant multifractality of the fluctuations in the Hall conductance. The maximum of $f(\alpha)$ is located at $\alpha_0 = 2.21$ (marked by an arrow in the figure), with $f(\alpha_0) = 1$; the maximum of $f(\alpha)$ provides the support dimension of the data series, which, in this case, is 1. A similar analysis of the fluctuations in G_{XX} yields that these too are multifractal (Supplemental Material [7], S8).

Note that the standard deviations of the small-amplitude fluctuations we analyze are at least an order of magnitude larger than the noise level measured at the IQH plateaus

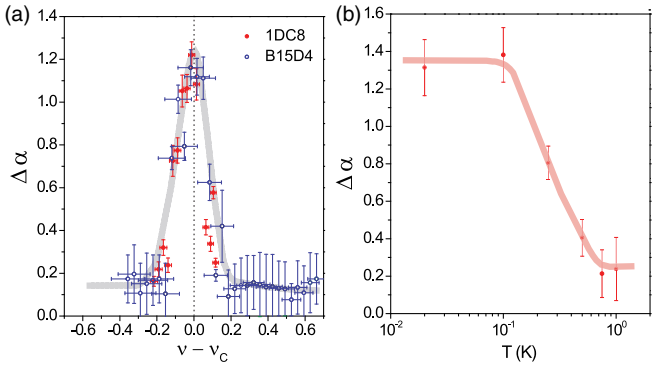

FIG. 4. (a) Plot of the spectral width $\Delta\alpha$ versus $\nu - \nu_C$ for the devices 1DC8 and B15D4. The vertical line marks the $\nu = 1 \leftrightarrow \nu = 2$ critical point. The gray-shaded curve is a guide to the eye. The error bars for the $\nu - \nu_C$ axis are calculated from the intrinsic impurity level in the device; the error bars in the $\Delta\alpha$ axis are derived from the error in calculating the slopes of the plots of $\log[F_q(s)]$ versus $\log[s]$ (Supplemental Material, S5). (b) Plot of $\Delta\alpha$ versus T for the device 1DC8, measured at $\nu = 1.6$. The red-shaded curve is a guide to the eye.

(Supplemental Material [7], S4). Consequently, our $f(\alpha)$ analysis is not contaminated by measurement noise. We also find that a random shuffling of the G_{XY} or the G_{XX} data series destroys its multifractality, suggesting that the origin of the multifractality lies in the long-range correlations picked up by charge carriers traversing through a hierarchical structure of the LDOS developed at IQH criticality (Supplemental Material [7], S6) [62].

In Fig. 4(a) we plot the spectral width $\Delta\alpha$ versus $\nu - \nu_C$ in the vicinity of the $\nu = 1 \leftrightarrow \nu = 2$ transition for both devices 1DC8 and B15D4; we find that the data for the two devices are quantitatively similar within error bars. The maxima in $\Delta\alpha$ is at $\nu \simeq \nu_C$, implying that the multifractality in G_{XY} peaks rather sharply near the $\nu = 1 \leftrightarrow \nu = 2$ critical point. At $\nu \simeq \nu_C$, $\Delta\alpha \simeq 1.3$, and it decreases sharply to $\Delta\alpha \sim 0.2$ at $|\nu - \nu_C| \sim 0.15$. The value of $\Delta\alpha$ away from $\nu = \nu_C$ is finite. We note that the critical states are confined to $E = E_C$ only in the thermodynamic limit. For a finite sized system, all states with localization length ξ larger than the system size appear to be extended, and the distribution of physical observables (including conductance fluctuations) is multifractal [30]. The divergence of ξ, away from $\nu = \nu_C$, is suppressed only algebraically and is governed by γ; so the critical states for a finite-sized system can indeed extend well beyond ν_C, albeit with algebraically reduced probability. Thus, our observation of a finite multifractality away from the critical point ν_C can be attributed to finite-size effects.

We note here that it is crucial to work with sufficiently high-mobility devices with a well-defined IQH critical point to observe this multifractality. Our primary objective was to study this multifractality at IQH criticality; the appearance of intervening fractional quantum Hall phases was, therefore, undesirable. The device widths were deliberately kept narrow to avoid the fractional quantum Hall phases. Keeping the device width small was also necessary to enhance the conductance fluctuations [63–65].

With increasing T, decoherence induced by inelastic thermal scattering reduces quantum interference and results in delocalization [66] leading to a monotonic decay in $\Delta\alpha$ [Fig. 4(b)]. Note again that the multifractality of the fluctuations in G_{XY} decreases well before the IQH plateaus disappear.

Finally, we discuss the possible effects of magnetic fields and disorder on our observations. The penetration length scale of the LDOS into the bulk of the material away from the IQH critical point is determined essentially by the magnetic length $l_B = h/(2\pi eB)$. For a magnetic field of 6 T ($l_B = 10$ nm) and 16 T ($l_B = 6.5$ nm), the magnetic lengths are extremely small as compared to the relevant length scales like either the sample width $W = 2$ μm or the localization length ξ (ξ in our devices is > 100 nm as estimated from the temperature scaling of conductance G_{XX} [67]). The multifractality of conductance fluctuations at high B (where the separation between the Landau levels is greater than either thermal or disorder broadening) is thus essentially independent of the magnetic field value (Supplemental Material [7], S9).

In the Hamiltonian of the IQH system, disorder enters as a random potential characterized by its amplitude and correlation length [23,68]. In hBN encapsulated graphene, the disorder potential arises primarily from the Coulomb interaction of the electrons with the fluctuating density of the dopant atoms [68,69]. The actual value of the amplitude $V(\mathbf{r})$ is unimportant as long as it is less than the cyclotron energy $E_{\rm cyc}$. The correlation length λ, on the other hand, is an important parameter: as long as $\lambda/l_B \gg 1$ (a condition satisfied in high-mobility two-dimensional systems in the presence of moderately strong B) the potential is smooth [21,41,68]. This leads to simple localization and confinement of the eigenstates (and LDOS) to a width $\sim l_B$ at the sample edge. It follows that the LDOS (and consequently the measured multifractality) will not be sensitive to the details of disorder as long as both $E_{\rm cyc}/V(\mathbf{r})$ and λ/l_B are $\gg 1$ [21,70]. Between the two devices, 1DC8 and B15D4, the defect density varies by a factor of 2, yet the multifractal behavior is essentially the same [see Fig. 4(a)]. In support of the statement that the disorder in our system is long-range, we note that the valley degeneracy is completely lifted at moderate values of B (see Supplemental Material [7]).

To conclude, we have presented the first experimental evidence for the multifractality of a transport property at a topological phase transition [3–6]. In particular, we have shown that conductance fluctuations at IQH $\nu = 1 \leftrightarrow \nu = 2$ and $\nu = 2 \leftrightarrow \nu = 3$ transitions in a high-mobility mesoscopic graphene device are multifractal. This multifractality gets rapidly suppressed as ν moves away from ν_C or as T is

increased. Although theoretical studies have shown the multifractality of eigenfunctions at this transition (see, e.g., Refs. [23,30,40,71–73]), there has been no experimental study hitherto on the multifractality of transport coefficients. We conjecture that similar multifractality of conductance fluctuations should also be present in (a) all IQH plateau-to-plateau transitions, (b) the fractional quantum Hall transitions, and (c) single-layer graphene devices. Our preliminary results support the conjectures (a) and (c). Our study also may provide an indirect route to access the evolution of the spatial distribution of the LDOS in such systems.

We thank S. S. Ray for fruitful discussions. A. B. acknowledges funding from DST (DST/SJF/PSA-01/2016-17). K. R. A. thanks CSIR, MHRD, Govt. of India for financial support. R. N. thanks MHRD, Govt. of India, for financial support. The authors thank NNfC, CeNSE, IISc for the device fabrication facilities and MNCF, CeNSE, IISc for the device characterization facilities. R. P. acknowledges support from CSIR, SERB, and the National Supercomputing Mission (India).

K. R. A. and R. N. contributed equally to the experiment.

*Present address: Department of Microtechnology and Nanoscience, Chalmers University of Technology, 412 96 Gothenburg, Sweden.

†Corresponding author.
aveek@iisc.ac.in

[1] *The Quantum Hall Effect*, edited by S. Girvin and R. Prange, Maryland Subseries: Based on Lectures at the University of Maryland, College Park (Springer-Verlag, Berlin, 1987).

[2] K. v. Klitzing, G. Dorda, and M. Pepper, New Method for High-Accuracy Determination of the Fine-Structure Constant Based on Quantized Hall Resistance, Phys. Rev. Lett. **45**, 494 (1980).

[3] J. E. Avron, R. Seiler, and B. Simon, Charge deficiency, charge transport and comparison of dimensions, Commun. Math. Phys. **159**, 399 (1994).

[4] D. J. Thouless, M. Kohmoto, M. P. Nightingale, and M. den Nijs, Quantized Hall Conductance in a Two-Dimensional Periodic Potential, Phys. Rev. Lett. **49**, 405 (1982).

[5] J. Bellissard, A. van Elst, and H. Schulz-Baldes, The noncommutative geometry of the quantum hall effect, J. Math. Phys. (N.Y.) **35**, 5373 (1994).

[6] J. E. Avron, D. Osadchy, and R. Seiler, A topological look at the quantum hall effect, Phys. Today **56**, No. 8, 38 (2003).

[7] See Supplemental Material at http://link.aps.org/supplemental/10.1103/PhysRevLett.129.186802 for more details of multifractal analysis calculations and device characteristics, which includes Refs. [8–16].

[8] L. Wang, I. Meric, P. Y. Huang, Q. Gao, Y. Gao, H. Tran, T. Taniguchi, K. Watanabe, L. M. Campos, D. A. Muller, J. Guo, P. Kim, J. Hone, K. L. Shepard, and C. R. Dean, One-dimensional electrical contact to a two-dimensional material, Science **342**, 614 (2013).

[9] F. Pizzocchero, L. Gammelgaard, B. S. Jessen, J. M. Caridad, L. Wang, J. Hone, P. Bøggild, and T. J. Booth, The hot pick-up technique for batch assembly of van der waals heterostructures, Nat. Commun. **7**, 11894 (2016).

[10] L. A. Ponomarenko, A. K. Geim, A. A. Zhukov, R. Jalil, S. V. Morozov, K. S. Novoselov, I. V. Grigorieva, E. H. Hill, V. V. Cheianov, V. I. Falko, K. Watanabe, T. Taniguchi, and R. V. Gorbachev, Tunable metal-insulator transition in double-layer graphene heterostructures, Nat. Phys. **7**, 958 (2011).

[11] J. W. Kantelhardt, Fractal and multifractal time series, in *Encyclopedia of Complexity and Systems Science*, edited by R. A. Meyers (Springer, New York, New York, NY, 2009), pp. 3754–3779.

[12] K. Hu, P. C. Ivanov, Z. Chen, P. Carpena, and H. E. Stanley, Effect of trends on detrended fluctuation analysis, Phys. Rev. E **64**, 011114 (2001).

[13] S. Faez, A. Strybulevych, J. H. Page, A. Lagendijk, and B. A. van Tiggelen, Observation of Multifractality in Anderson Localization of Ultrasound, Phys. Rev. Lett. **103**, 155703 (2009).

[14] F. Evers, A. Mildenberger, and A. D. Mirlin, Multifractality of wave functions at the quantum Hall transition revisited, Phys. Rev. B **64**, 241303(R) (2001).

[15] T. Terao, T. Nakayama, and H. Aoki, Multifractality of the quantum Hall wave functions in higher Landau levels, Phys. Rev. B **54**, 10350 (1996).

[16] I. A. Gruzberg, A. D. Mirlin, and M. R. Zirnbauer, Classification and symmetry properties of scaling dimensions at anderson transitions, Phys. Rev. B **87**, 125144 (2013).

[17] Q. Niu and D. J. Thouless, Quantum hall effect with realistic boundary conditions, Phys. Rev. B **35**, 2188 (1987).

[18] C. W. J. Beenakker, Random-matrix theory of quantum transport, Rev. Mod. Phys. **69**, 731 (1997).

[19] R. B. Laughlin, Quantized hall conductivity in two dimensions, Phys. Rev. B **23**, 5632 (1981).

[20] A. Giuliani, V. Mastropietro, and M. Porta, Quantization of the interacting hall conductivity in the critical regime, J. Stat. Phys. **180**, 332 (2020).

[21] S. Ilani, J. Martin, E. Teitelbaum, J. H. Smet, D. Mahalu, V. Umansky, and A. Yacoby, The microscopic nature of localization in the quantum hall effect, Nature (London) **427**, 328 (2004).

[22] A. L. R. Barbosa, T. H. V. de Lima, I. R. R. Gonzalez, N. L. Pessoa, A. M. S. Macedo, and G. L. Vasconcelos, Turbulence Hierarchy and Multifractality in the Integer Quantum Hall Transition, Phys. Rev. Lett. **128**, 236803 (2022).

[23] B. Huckestein, Scaling theory of the integer quantum hall effect, Rev. Mod. Phys. **67**, 357 (1995).

[24] W. Li, C. L. Vicente, J. S. Xia, W. Pan, D. C. Tsui, L. N. Pfeiffer, and K. W. West, Scaling in Plateau-to-Plateau Transition: A Direct Connection of Quantum Hall Systems with the Anderson Localization Model, Phys. Rev. Lett. **102**, 216801 (2009).

[25] J. Chalker, *Aspects Topologiques de la Physique en Basse Dimension. Topological Aspects of Low Dimensional Systems* (Springer, New York, 1999).

[26] J. T. Chalker and G. J. Daniell, Scaling, Diffusion, and the Integer Quantized Hall Effect, Phys. Rev. Lett. **61**, 593 (1988).

[27] M. B. Hastings and S. Michalakis, Quantization of hall conductance for interacting electrons on a torus, Commun. Math. Phys. **334**, 433 (2015).
[28] J. E. Avron, D. Osadchy, and R. Seiler, A topological look at the quantum hall effect, Phys. Today **56**, No. 8, 38 (2003).
[29] F. Evers and A. D. Mirlin, Anderson transitions, Rev. Mod. Phys. **80**, 1355 (2008).
[30] M. Janssen, Multifractal analysis of broadly-distributed observables at criticality, Int. J. Mod. Phys. B **08**, 943 (1994).
[31] T. Nakayama and K. Yakubo, *Fractal Concepts in Condensed Matter Physics*, Springer Series in Solid-State Sciences (Springer, Berlin, Heidelberg, 2013).
[32] B. Huckestein and B. Kramer, One-Parameter Scaling in the Lowest Landau Band: Precise Determination of the Critical Behavior of the Localization Length, Phys. Rev. Lett. **64**, 1437 (1990).
[33] B. Huckestein and L. Schweitzer, Multifractal behavior and scaling in disordered mesoscopic QHE-systems, Physica (Amsterdam) **191A**, 406 (1992).
[34] B. Huckestein and L. Schweitzer, Relation between the Correlation Dimensions of Multifractal Wave Functions and Spectral Measures in Integer Quantum Hall Systems, Phys. Rev. Lett. **72**, 713 (1994).
[35] K. R. Amin, S. S. Ray, N. Pal, R. Pandit, and A. Bid, Exotic multifractal conductance fluctuations in graphene, Commun. Phys. **1**, 1 (2018).
[36] G. Benenti, G. Casati, I. Guarneri, and M. Terraneo, Quantum Fractal Fluctuations, Phys. Rev. Lett. **87**, 014101 (2001).
[37] G. Casati, I. Guarneri, and G. Maspero, Fractal Survival Probability Fluctuations, Phys. Rev. Lett. **84**, 63 (2000).
[38] A. Facchini, S. Wimberger, and A. Tomadin, Multifractal fluctuations in the survival probability of an open quantum system, Physica (Amsterdam) **376A**, 266 (2007).
[39] A. Espinosa-Champo and G. G. Naumis, Multifractal wavefunctions of charge carriers in graphene with folded deformations, ripples, or uniaxial flexural modes: Analogies to the quantum hall effect under random pseudomagnetic fields, J. Vac. Sci. Technol. B **39**, 062202 (2021).
[40] D. H. Cobden, C. H. W. Barnes, and C. J. B. Ford, Fluctuations and Evidence for Charging in the Quantum Hall Effect, Phys. Rev. Lett. **82**, 4695 (1999).
[41] B. E. Feldman, B. Krauss, J. H. Smet, and A. Yacoby, Unconventional sequence of fractional quantum hall states in suspended graphene, Science **337**, 1196 (2012).
[42] A. Tsinober, Turbulence: The legacy of a. n. kolmogorov. by u. frisch. cambridge university press, J. Fluid Mech. **317**, 407 (1996).
[43] M. Ghil, R. Benzi, and G. Parisi, *Turbulence and Predictability in Geophysical Fluid Dynamics and Climate Dynamics* (North Holland, Amsterdam, 1985), Vol. 88.
[44] R. Benzi, G. Paladin, G. Parisi, and A. Vulpiani, On the multifractal nature of fully developed turbulence and chaotic systems, J. Phys. A **17**, 3521 (1984).
[45] R. Pandit, P. Perlekar, and S. S. Ray, Statistical properties of turbulence: An overview, Pramana **73**, 157 (2009).
[46] N. Pal, P. Perlekar, A. Gupta, and R. Pandit, Binary-fluid turbulence: Signatures of multifractal droplet dynamics and dissipation reduction, Phys. Rev. E **93**, 063115 (2016).
[47] S. Buldyrev, N. Dokholyan, A. Goldberger, S. Havlin, C.-K. Peng, H. Stanley, and G. Viswanathan, Analysis of dna sequences using methods of statistical physics, Physica (Amsterdam) **249A**, 430 (1998).
[48] M. Zeng, X.-N. Zhang, J.-H. Li, and Q.-H. Meng, The scaling properties of high-frequency wind speed records based on multiscale multifractal analysis., Acta Phys. Pol. B **47** (2016).
[49] R. N. Mantegna, H. E. Stanley, and N. A. Chriss, An introduction to econophysics: Correlations and complexity in finance, Phys. Today **53**, No. 12, 70 (2000).
[50] J. Gieraltowski, J. J. Zebrowski, and R. Baranowski, Multiscale multifractal analysis of heart rate variability recordings with a large number of occurrences of arrhythmia, Phys. Rev. E **85**, 021915 (2012).
[51] P. C. Ivanov, L. A. N. Amaral, A. L. Goldberger, S. Havlin, M. G. Rosenblum, Z. R. Struzik, and H. E. Stanley, Multifractality in human heartbeat dynamics, Nature (London) **399**, 461 (1999).
[52] K. Ivanova, M. Ausloos, E. E. Clothiaux, and T. P. Ackerman, Break-up of stratus cloud structure predicted from non-brownian motion liquid water and brightness temperature fluctuations, Europhys. Lett. **52**, 40 (2000).
[53] J. Sutradhar, S. Mukerjee, R. Pandit, and S. Banerjee, Transport, multifractality, and the breakdown of single-parameter scaling at the localization transition in quasiperiodic systems, Phys. Rev. B **99**, 224204 (2019).
[54] B. Jack, F. Zinser, E. J. Konig, S. N. P. Wissing, A. B. Schmidt, M. Donath, K. Kern, and C. R. Ast, Visualizing the multifractal wave functions of a disordered two-dimensional electron gas, Phys. Rev. Res. **3**, 013022 (2021).
[55] J. E. Barrios-Vargas and G. G. Naumis, Electron localization in disordered graphene for nanoscale lattice sizes: Multifractal properties of the wavefunctions, 2D Mater. **1**, 011009 (2014).
[56] L. G. C. S. Sa, A. L. R. Barbosa, and J. G. G. S. Ramos, Conductance peak density in disordered graphene topological insulators, Phys. Rev. B **102**, 115105 (2020).
[57] N. L. Pessoa, A. L. R. Barbosa, G. L. Vasconcelos, and A. M. S. Macedo, Multifractal magnetoconductance fluctuations in mesoscopic systems, Phys. Rev. E **104**, 054129 (2021).
[58] C. Rubio-Verdu, A. M. Garcia-Garcia, H. Ryu, D.-J. Choi, J. Zaldivar, S. Tang, B. Fan, Z.-X. Shen, S.-K. Mo, J. I. Pascual, and M. M. Ugeda, Visualization of multifractal superconductivity in a two-dimensional transition metal dichalcogenide in the weak-disorder regime, Nano Lett. **20**, 5111 (2020).
[59] K. Zhao *et al.*, Disorder-induced multifractal superconductivity in monolayer niobium dichalcogenides, Nat. Phys. **15**, 904 (2019).
[60] S. Das Sarma, S. Adam, E. H. Hwang, and E. Rossi, Electronic transport in two-dimensional graphene, Rev. Mod. Phys. **83**, 407 (2011).
[61] A. Kou, B. E. Feldman, A. J. Levin, B. I. Halperin, K. Watanabe, T. Taniguchi, and A. Yacoby, Electron-hole asymmetric integer and fractional quantum hall effect in bilayer graphene, Science **345**, 55 (2014).
[62] J. W. Kantelhardt, S. A. Zschiegner, E. Koscielny-Bunde, S. Havlin, A. Bunde, and H. Stanley, Multifractal detrended

fluctuation analysis of nonstationary time series, Physica (Amsterdam) **316A**, 87 (2002).

[63] C. Beenakker and H. van Houten, *Semiconductor Heterostructures and Nanostructures*, edited by H. Ehrenreich and D. Turnbull, Solid State Physics (Academic Press, New York, 1991), Vol. 44, pp. 1–228.

[64] B. Scannell, T. Martin, M. Fairbanks, H. Linke, C. Marlow, T. Fromhold, C. Brown, K. Ishibashi, and R. Taylor, Quantum conductance fluctuations in semiconductor devices, Curr. Appl. Phys. **8**, 332 (2008).

[65] C. V. Brown, A. K. Geim, T. J. Foster, C. J. G. M. Langerak, and P. C. Main, Mesoscopic fluctuations in high magnetic fields: Change in behavior due to boundary diffusion, Phys. Rev. B **47**, 10935 (1993).

[66] D. Polyakov, Quantum hall effect at finite temperatures, arXiv:cond-mat/9608013.

[67] N. A. Dodoo-Amoo, K. Saeed, D. Mistry, S. P. Khanna, L. Li, E. H. Linfield, A. G. Davies, and J. E. Cunningham, Non-universality of scaling exponents in quantum hall transitions, J. Phys. Condens. Matter **26**, 475801 (2014).

[68] D. Rhodes, S. H. Chae, R. Ribeiro-Palau, and J. Hone, Disorder in van der waals heterostructures of 2d materials, Nat. Mater. **18**, 541 (2019).

[69] C. R. Dean, A. F. Young, I. Meric, C. Lee, L. Wang, S. Sorgenfrei, K. Watanabe, T. Taniguchi, P. Kim, K. L. Shepard, and J. Hone, Boron nitride substrates for high-quality graphene electronics, Nat. Nanotechnol. **5**, 722 (2010).

[70] T. Champel and S. Florens, High magnetic field theory for the local density of states in graphene with smooth arbitrary potential landscapes, Phys. Rev. B **82**, 045421 (2010).

[71] E. Peled, D. Shahar, Y. Chen, D. L. Sivco, and A. Y. Cho, Observation of a Quantized Hall Resistivity in the Presence of Mesoscopic Fluctuations, Phys. Rev. Lett. **90**, 246802 (2003).

[72] E. Peled, D. Shahar, Y. Chen, E. Diez, D. L. Sivco, and A. Y. Cho, Near-Perfect Correlation of the Resistance Components of Mesoscopic Samples at the Quantum Hall Regime, Phys. Rev. Lett. **91**, 236802 (2003).

[73] D. H. Cobden and E. Kogan, Measurement of the conductance distribution function at a quantum hall transition, Phys. Rev. B **54**, R17316(R) (1996).